ACS Appl. Mater. Interfaces, 2017, 9 (3), pp 3156–3160

DOI: 10.1021/acsami.6b14372

Robust Interfacial Exchange Bias and Metal–Insulator Transition Influenced by the $LaNiO_3$ Layer Thickness in $La_{0.7}Sr_{0.3}MnO_3/LaNiO_3$ Superlattices

Guowei Zhou,[†,‡] Cheng Song,[∥] Yuhao Bai,[†,‡] Zhiyong Quan,[†,‡] Fengxian Jiang,[†,‡] Wenqing Liu,[§,#] Yongbing Xu,[§] Sarnjeet Dhesi,[✣] and Xiaohong Xu[*†,‡]*

[†] School of Chemistry and Materials Science, Key Laboratory of Magnetic Molecules and Magnetic Information Materials, Ministry of Education, Shanxi Normal University, Linfen 041004, China

[‡] Research Institute of Materials Science, Shanxi Normal University, Linfen 041004, China

[∥] Key Laboratory of Advanced Materials (MOE), School of Materials Science and Engineering, Tsinghua University, Beijing 100084, China

[§] Spintronics and Nanodevice Laboratory, Department of Electronics, University of York, York YO10 5DD, U.K.

[#] Department of Electronic Engineering, Royal Holloway, University of London, Egham, Surrey, TW20 0EX, U.K.

[✣] Diamond Light Source, Didcot OX11 0DE, United Kingdom

ABSTRACT: Artificial heterostructures based on $LaNiO_3$ (LNO) have been widely investigated with the aim to realize the insulating antiferromagnetic state of LNO. In this work, we have grown $[(La_{0.7}Sr_{0.3}MnO_3)_5\text{-}(LaNiO_3)_n]_{12}$ superlattices on (001)-oriented $SrTiO_3$ substrates by pulsed laser deposition and observed an unexpected exchange bias effect in field-cooled hysteresis loops. Through X-ray absorption spectroscopy and magnetic circular dichroism experiments, we found that the charge transfer at the interfacial Mn and Ni ions can induce a localized magnetic moment. A remarkable increase of exchange bias field and a transition from metal to insulator were simultaneously observed upon decreasing the thickness of the LNO layer, indicating the antiferromagnetic insulator state in 2 unit cells (u.c.) LNO ultrathin layers. The robust exchange bias of 745 Oe in the superlattice is caused by an interfacial localized magnetic moment and an antiferromagnetic state in the ultrathin LNO layer pinning the ferromagnetic $La_{0.7}Sr_{0.3}MnO_3$ layers together. Our results demonstrate that artificial interface engineering is a useful method to realize novel magnetic and transport properties.

KEYWORDS: *exchange bias, charge transfer, metal-insulator transition, LNO thickness, superlattices*

1. INTRODUCTION

Transition metal-oxides interfaces exhibit a great amount of interesting phenomena such as high temperature superconductivity, metal-insulator transitions, exchange bias coupling, and magnetoelectric coupling[1-4]. These novel properties are considered to be closely related to the interfacial strong correlation between the charge, spin, orbital, and lattice degrees of freedom. The artificial deposition of heterostructures is an effective way to investigate the exceptional states which are completely different from those of the corresponding bulk materials[5,6]. The magnetic properties of oxide heterostructures that composed of ruthenates, cuprates, and manganites have been investigated abundantly, while the research of nickelates heterostructure remains relatively less attention[7-9]. The nickelate oxides of composition RNiO$_3$ with smaller lanthanide ions (R≠La) exhibit a metal-insulator transition accompanied by the transition from paramagnetic to antiferromagnetic as a function of temperature, except for LaNiO$_3$ (LNO), which always behave as a paramagnetic metal at all temperatures in its bulk form[10,11]. In recent years, the metal-insulator transition has been observed in LaNiO$_3$ ultrathin films and in LaNiO$_3$/LaAlO$_3$ superlattices[12-15]. The unexpected exchange bias (EB) effect can be found in (111)-oriented superlattices structures and while it is not present in (001)-oriented structures, composed of ferromagnetic (FM) LaMnO$_3$ and paramagnetic (PM) LaNiO$_3$[16-21]. It is well known that (001) oriented superlattices with lower energy are easily epitaxially deposited as opposed to the (111) oriented structures, and the interrelation between exchange bias and transport properties in (001)-oriented LNO-based superlattices still needs to be thoroughly understood.

In this paper, we employed La$_{0.7}$Sr$_{0.3}$MnO$_3$ (LSMO) fixed as 5 u.c. and paramagnetic metallic LaNiO$_3$ (LNO) materials varying from 2 u.c. to 7 u.c. to prepare the superlattices on (001) SrTiO$_3$ substrates. In such superlattices, the charge transfer between Mn and Ni ions results in the localized super-exchange ferromagnetism at the interface. Upon decreasing the thickness of the LNO layer, the transition from metal to insulator and the remarkable increase in the exchange bias suggest that an insulating antiferromagnetic state appears in ultrathin

LNO layer. The robust EB effect can be observed in LSMO (5)/LNO (2) superlattices due to the pinning of the ferromagnetic LSMO by the localized magnetic moment at the interface and the antiferromagnetic state in LNO layer, and this effect is almost one order of magnitude higher than in an (111)-oriented LMO/LNO superlattice[16].

2. EXPERIMENTAL

The epitaxial fabrication of $[(La_{0.7}Sr_{0.3}MnO_3)_5\text{-}(LaNiO_3)_n]_{12}$ superlattices (SLs) were grown on atomically flat $SrTiO_3$ (001) substrates (see Figure S1). Here, *n* is the number of LNO unit cells which can be set to 2, 4 or 7. The LSMO layer is always in an insulating ferromagnetic state[22]. The SLs were grown by a Pulsed Laser Deposition (PLD) apparatus equipped with *in situ* Reflection High Energy Electron Diffraction (RHEED) at 725 °C at an oxygen pressure of 100 mTorr to avoid any change in oxygen vacancies density at the interface. After the growth, the samples were annealed in a 300 Torr oxygen atmosphere *in situ* for one hour in order to improve their quality and reduce their inherent oxygen deficit, then cooled down to room temperature. The crystal structure and epitaxy of three different SLs were determined by X-Ray Diffraction (XRD). To study the structure quality and the interfacial abruptness of the samples, a typical High-Angle Annular Dark Field Scanning Transmission Electron Microscope (HAADF-STEM) was employed, with atomic resolution and equipped with aberration corrections. X-ray Absorption Spectroscopy (XAS) measurements in Total Electron Yield mode (TEY), were performed *ex situ* (E//a) at Beamline BL12B-a of the National Synchrotron Radiation Laboratory (NSRL), China[23], as a surface sensitive technique at room temperature. X-ray Magnetic Circular Dichroism (XMCD) measurements in Florescence Yield mode (FY), were performed at 1.6 K on Beamline 106 at the Diamond Light Source[24], as a bulk sensitive technique, in grazing incidence conditions (E//c) with a 30° angle between the X-ray beam direction and the sample. Magnetic measurements were performed with a Vibrating Sample Magnetometer in PPMS (PPMS-VSM) with in-plan applied magnetic field, and hysteresis curves were obtained after subtracting the diamagnetic background. Transport measurements were performed in the Van der Pauw four-point probe configuration with a Quantum Design Physical Properties Measurement System (PPMS).

3. RESULTS AND DISCUSSION

Typical XRD patterns are shown in Figure 1a, revealing a high quality growth in the expected (001) orientation for all the samples. Moreover, the observation of satellite peaks in the SLs suggests a high degree of interface abruptness between the LSMO and LNO layers. The distance between adjacent satellite peaks increases as the LNO thickness decrease, as expected for Bragg reflections[25]. Figure 1b, displays the result of a typical HAADF-STEM image in order to directly illustrate the structural quality and interfacial abruptness of the samples. The image intensity in the HAADF image is proportional to $\sim Z^{1.7}$, where Z is the atomic number. Therefore, the brighter features indicate the heavier elements. Due to the strontium atom substituting a lanthanum atom in its lattice site, La atoms (Z=57) are brighter than La/Sr atoms (Z=57/38), while the weaker spots in between indicate Ni (Z=28) and Mn (Z=25) atoms columns with similar intensities (see Figure S2). The total thickness of the SL is measured to be 31.2 nm, which is close to the expected value of 32.4 nm and within the expected uncertainty of the measurement. The image demonstrates the high quality of the superlattices, due to the excellent epitaxial registry across interfaces and to the absence of secondary phases or amorphous layers.

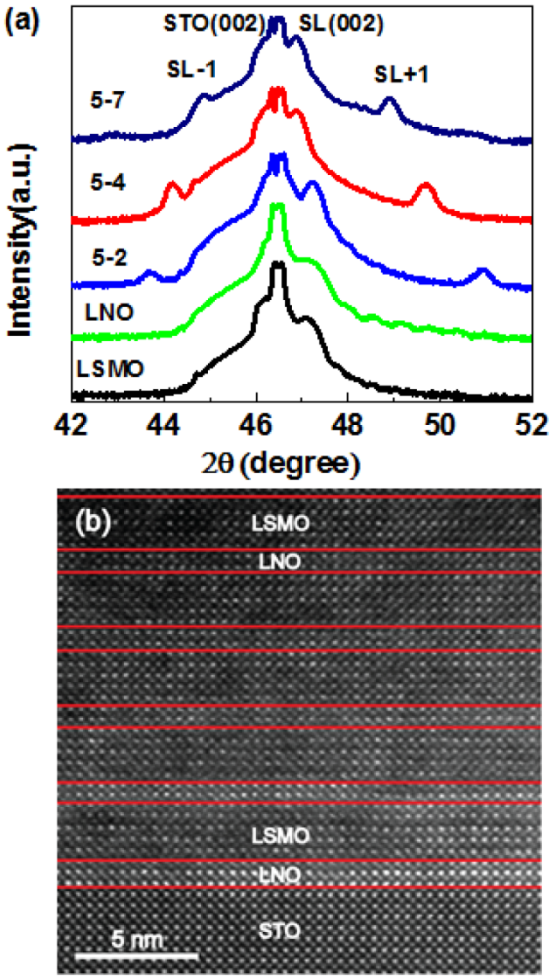

Figure 1. (Color online) (a) XRD patterns for three different SLs, LNO and LSMO single layer on STO substrate. (b) Typical HAADF-STEM image of the (5-2) SL.

Figure 2a displays the magnetic hysteresis loops of (5-2) SL, obtained at 5 K after a +0.5 T field-cooling (FC) and zero filed cooling (ZFC) procedure from room temperature. The hysteresis loop after the FC process exhibits a significant shift along the magnetic field axis towards negative field values, compared with the zero field-cooling. This feature indicates that the presence of the exchange bias effect in the (5-2) SL. According to previous research, the coercivity increases when the exchange bias effect appears[26]. The values of the EB field (H_{EB}) and of the coercivity (H_C) are respectively given by $H_{EB}=|H_+ +H_-|/2$ and $H_C=|H_+-H_-|/2$, where H_+ and H_- denote the right and left values of coercivity as the magnetization goes to zero. Our measured values for H_+ and H_- are -2673 Oe and 1183 Oe, respectively. In this loop, the value of H_{EB} is 745 Oe and H_C is 1865 Oe, which is several

orders of magnitude higher than what previous reported for LSMO/LNO bilayers[27,28]. The temperature dependence of exchange bias field and coercivity for the (5-2) SL is illustrated in the inset of Figure 2a. H_{EB} rapidly decreases as the temperature increases, finally becoming zero at 18 K, which is known as the conventional blocking temperature (T_B) [29]. The coercivity also exhibits a continuous decrease with increasing temperature, in agreement with similar results obtained on other manganite superlattice[30]. Figure 2b summarizes the results of the coercivity and exchange bias field measurements for (5-2), (5-4), and (5-7) SLs, performed at 5 K after a +0.5 T field cooling. H_C decreases from 1865 Oe to 896 Oe and H_{EB} reduces from 745 Oe to 64 Oe as the LNO layer increases from 2 u.c. to 7 u.c., respectively. The origin of the interfacial exchange bias and its dependence on the LNO thickness are discussed in the following sections.

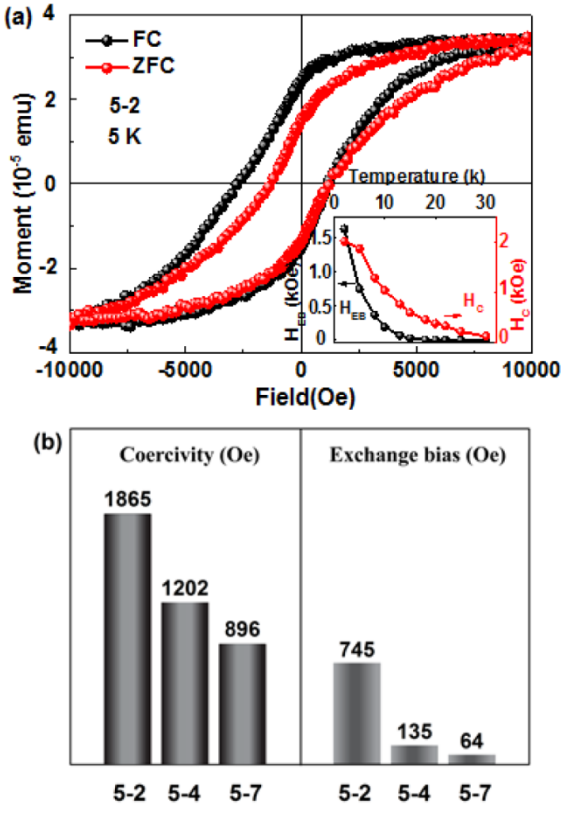

Figure 2. (Color online) (a) Magnetic hysteresis loops at 5 K for a $(5\text{-}2)_{12}$ SL after field-cooling from room temperature in a +0.5 T field (black) and with zero field cooling (red). Inset: the temperature dependence of H_{EB} and H_C for the $(5\text{-}2)_{12}$ superlattices. (b) Coercivity and exchange bias as a function of the number of unit cells for (5-2), (5-4), and (5-7) SLs.

X-ray Absorption Spectra were measured in TEY mode with photon polarization parallel (E//a) to the samples, in order to determine the valence states of Mn and Ni ions near the interface. The information on the unoccupied Mn 3*d* state and the related Mn valence state can be deduced by the Mn *L*-edge in the absorption spectra, of resulting from Mn $2p_{3/2,1/2} \rightarrow 3d$ dipole transitions[31]. Due to the spin-orbital interaction of Mn 2*p* states, the spectrum is split into two broad multiplets, the L_3 (Mn $2p_{3/2} \rightarrow 3d$) edge at ~642 eV and the L_2 (Mn $2p_{1/2} \rightarrow 3d$) edge at ~653 eV. Figure 3a displays the XAS spectra measured at Mn $L_{3,2}$ edges for (5-2), (5-4) and (5-7) SLs, and the single LSMO for comparison. According to the results of XAS, we find that the L_3 peak of the SLs is shifted towards higher energy values with respect to the single LSMO, indicating a stronger Mn^{4+} character in the superlattices[27]. Conversely, the L_3 peak of Mn does not shift among the three different SLs. XAS spectra were also acquired at the Ni $L_{3,2}$ edges (see Figure S3), nevertheless, the L_2 edge intensity of Ni is too weak to resolve energy shifts, and the L_3 edge overlaps with the La M_4 edge[20]. In order to characterize the chemical state of Ni, X-ray photoelectron spectroscopy (XPS) was employed and the results are shown in Figure 3b. The peak1 around 854 eV is identified as the Ni $2p_{3/2}$ peak, and its shift towards lower energies in SLs points at a lower Ni valence states at the interface. Combining the increase of Mn valence at the interface as deduced by the position of the Mn *L*-edge XAS with this decrease of Ni valence, it is quite natural to hypothesize that charge transfer occurs from Mn ions to Ni ions at the SLs interface.

In the interfacial coupling, the hybridization between the Mn and Ni 3*d* orbitals provides useful information on the O 2*p* orbitals variation[32]. The O *K*-edge is mainly influenced by the unoccupied O 2*p* states via O $1s \rightarrow 2p$ transitions. According to results available in the literature[33], the origin of the broad peak at 544 eV is attributed to electronic bands of Mn 4*sp* and La 6*sp*, while the one at 536 eV is related to a La 5*d* orbital. In particular, the peak marked by a thick arrow at 533 eV that is primarily illustrating the O 2*p* hybridized with mixed electrons of Mn or Ni ions[34]. As shown in Figure 3c, the peak at 533 eV is distinctly visible in the SLs and its intensity increases monotonically as the LNO thickness decreases, indicating the rising degree of hybridization between Mn and Ni ions as Mn^{3+}-$Ni^{3+} \rightarrow Mn^{4+}$-$Ni^{2+}$ occurring in La_2NiMnO_6 double perovskite[35]. As the Fermi level of

LSMO is higher than that of the LNO layer[18], electrons transfer from Mn to Ni sites easily as depicted in Figure 3d.

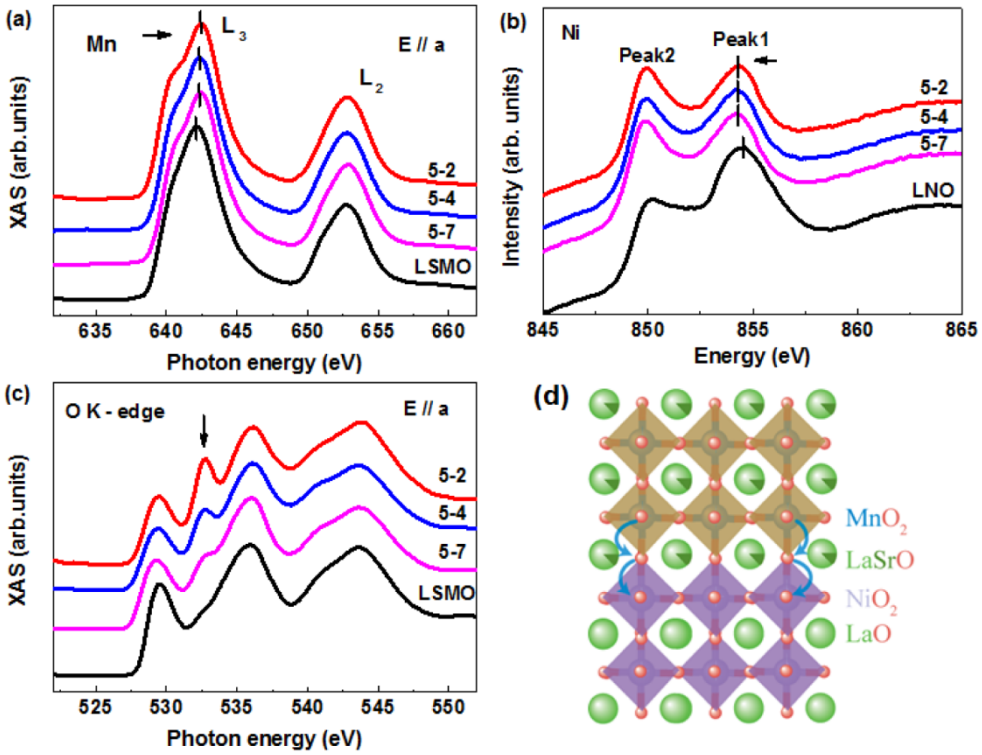

Figure 3. (Color online) (a) XAS curves of the Mn *L* edge for (5-2), (5-4), and (5-7) SLs. The spectrum for a single LSMO reference sample is shown for comparison (black line). The vertical line marks the position of the XAS peaks and has been shifted for clarity. (b) Ni 2*p* XPS spectra of different samples. The peak labeled as "peak1" is composed of Ni $2p_{3/2}$. (c) Oxygen *K*-edge absorption spectra of different samples measured in TEY mode with photon polarization perpendicular to the sample plane. The vertical offset in all spectra is applied to allow better visualization. (d) Schematic view of the interfacial charge transfer mechanism from Mn to Ni ions.

In order to measure the interfacial magnetic signal, we employed the FY mode with photon polarization at 30° grazing incidence to the sample (with E//c) to measure the (5-2) SL in an applied field of 6 T at 1.6 K. Figure 4a and 4b present the measured XMCD at the Mn and Ni *L* edges, respectively. The XMCD signal is obtained from the discrepancy with the XAS signal in right (μ_+) and left (μ_-) applied field along the X-ray propagation direction. The Mn and Ni L_2 edges have the same sign, which demonstrates that the net spin moments of both layers are aligned parallel to each other. This is expected to be a ferromagnetic

configuration arising either from double-exchange or super exchange interaction[36]. If double-exchange ferromagnetism is observed in the SLs, an increase of metallicity as a function of temperature is expected, which cannot occur in this superlattice as illustrated in Figure 5. According to the Goodenough-Kanamori rules[37], the coupling between Mn^{4+} and Ni^{2+} cations is expected to be mediated by ferromagnetic super-exchange. By simultaneously considering the XAS and XMCD spectra characters, we can state that charge transfer between Mn and Ni ions at the interface favors the super-exchange ferromagnetic coupling to reveal the localized magnetic moment. As a result, the interfacial exchange bias is due to the pinning of the ferromagnetic LSMO layer by the localized magnetic moment. However, the exchange bias drastically changes from 745 Oe to 64 Oe as the LNO thickness increases from 2 u.c. to 7 u.c., and no significant shifts of the Mn L_3 edge absorption peak and of the Ni $2p_{3/2}$ edge are observed in different SLs. This phenomenon suggests there is another driving mechanism behind the larger exchange bias value in ultrathin SLs, which needs to be investigated by further research.

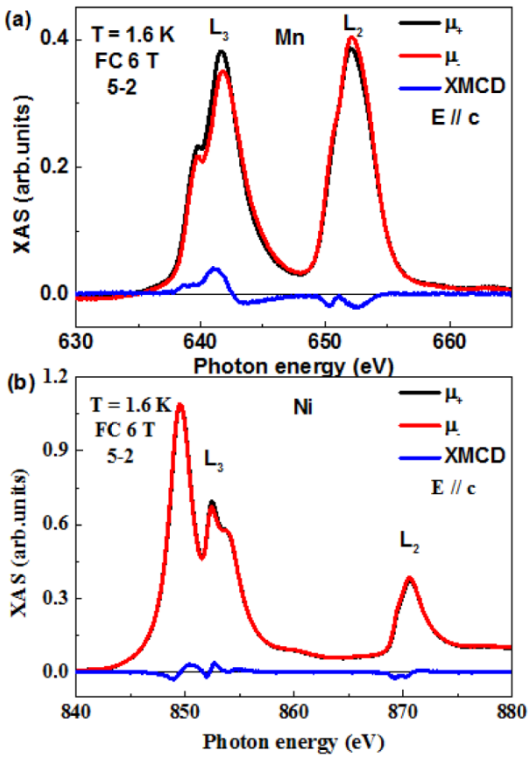

Figure 4. (Color online) XAS and XMCD spectra with photon polarization at 30° grazing incidence to the sample plane in FY mode for (5-2) SL at (a) Mn and (b) Ni $L_{3,2}$ edges measured at 6 T and 1.6 K.

Figure 5 presents the in-plane resistance curves of three different SLs as a function of temperature. The SLs undergo a metal-insulator transition as the thickness of LNO layers decreases. The difference in resistance as a result of this transition is as large as six orders of magnitude. At the same time, the exchange bias sharply increases from 64 Oe to 745 Oe as the number of LNO layers decreases. According to the previous literature[38], the insulating ground state of all perovskite nickelates $RNiO_3$ is in an antiferromagnetic configuration, which makes LNO an exception within the perovskite family, failing to exhibit this order in its bulk. Similarly, the correlation magnetic and transport properties in LSMO/LNO superlattices are also affected by the thickness of the LNO layer, which provides a useful evidence to support the antiferromagnetic order in ultrathin LNO layers as other nickelates. Gibert *et al.* have recently reported a dimensionality-induced magnetic order, in $LaMnO_3/LaNiO_3$ superlattices, as an antiferromagnetic structure emerged in an LNO layer[21]. Therefore, the larger exchange bias in (5-2) superlattices is attributed to the localized magnetic moment at the interface and to the antiferromagnetic order in the ultrathin LNO layer pinning the ferromagnetic LSMO layer together.

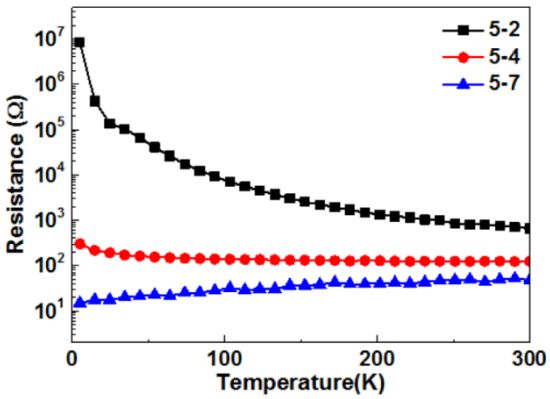

Figure 5. (Color online) Temperature dependence of the resistance for a series of LNO thickness ranging from 2 to 7 u.c..

4. CONCLUSIONS

To summarize, an unexpected exchange bias is observed in (001)-oriented LSMO/LNO superlattices. XAS and XMCD experiments suggest the occurrence of charge transfer and the

presence of a localized magnetic moment at interfacial Mn and Ni ions. The exchange bias sharply increases from 64 Oe to 745 Oe, and the electrical transport properties accordingly change from a metal-like to insulating behavior as the thickness of LNO layer decrease from 7 u.c. to 2 u.c.. This competition between magnetic and transport properties in superlattices indicates that the antiferromagnetic insulating state exists in ultrathin LNO layers. This novel phenomenon occurring at the interfaces between paramagnetic and ferromagnetic material, opens the way for tailoring the properties of complex oxides via artificial interface engineering.

■ *ASSOCIATED CONTENT*

Supporting Information

The Supporting Information is available free of charge on the ACS Publications website. RHEED patterns for the $(5\text{-}2)_{12}$ superlattices before and after the deposition, partial oscillating curve of the $(5\text{-}2)_{12}$ SLs, AFM image for the etched $SrTiO_3$ substrate, integral HADDF-STEM of (5-2) SLs, and XAS scans at Ni *L* edge.

■ *AUTHOR INFORMATION*

Corresponding Author

*E-mail: xuxh@dns.sxnu.edu.cn

Notes

The authors declare no competing financial interest.

■ *ACKNOWLEDGMENTS*

We thank Wensheng Yan for the XAS measurement at Beamline BL12-a in National Synchrotron Radiation Laboratory (NSRL). Diamond light source is acknowledged to beamline 06 under SI12664. The work is financially supported by National High Technology Research and Development Program of China (863 program, No. 2014AA032904), NSFC

(Nos. 51025101, 11274214, 61434002 and 51571136), and the Special Funds of Shanxi Scholars Program, the Ministry of Education of China (Nos. IRT1156 and 20121404130001) and Sanjin scholar project.

REFERENCES

(1) Bhattacharya, A.; May, S. J. Magnetic Oxide Heretostructures. *Annu. Rev. Mater. Res.* **2014,** *44,* 65-90.

(2) Hwang, H. Y.; Iwasa, Y.; Kawasaki, M.; Kiemer, B.; Nagaosa, N.; Tokura, Y. Emergent Phenomena at Oxide Interfaces. *Nat. Mater.* **2012,** *11,* 103-113.

(3) Nogués, J.; Schuller, I. K. Exchange Bias. *J. Magn. Magn. Mater.* **1999,** *192,* 203-232.

(4) Zubko, P.; Gariglio, S.; Gabay, M.; Ghosez, P.; Triscone, J. M. Interface Physics in Complex Oxide Heterostructures. *Annu. Rev. Condens. Matter Phys.* **2011,** *2,* 141-165.

(5) Ohtomo, A.; Hwang, H. Y. A High-mobility Electron Gas at the $LaAlO_3/SrTiO_3$ Heterointerface. *Nature* **2004,** *427*, 423-426.

(6) Takahashi, K. S.; Kawasaki, M.; Tokura, Y. Interface Ferromagnetism in Oxide Superlattices of $CaMnO_3/CaRuO_3$. *Appl. Phys. Lett.* **2001,** *79,* 1324.

(7) Tian, Y. F.; Lebedev, O. I.; Roddatis, V. V.; Lin, W. N.; Ding, J. F.; Hu, S. J.; Yan, S. S.; Wu, T. Interfacial Magnetic Coupling in Ultrathin all-manganite $La_{0.7}Sr_{0.3}MnO_3$-$TbMnO_3$ Superlattices. *Appl. Phys. Lett.* **2014,** *104,* 152404.

(8) Ding, J. F.; Cossu, F.; Lebedev, O. I.; Zhang, Y. Q.; Zhang, Z. D.; Schwingenschlögl, U.; Wu, T. Manganite/Cuprate Superlattice as Artificial Reentrant Spin Glass. *Adv. Mater. Interfaces* **2016**, *3*, 1500676.

(9) Ziese, M.; Vrejoiu, I. Properties of Manganite/Ruthenate Superlattices with Ultrathin Layers. *Phys. Status Solidi PRL* **2013**, *7*, 243-257.

(10) Lacorre, P.; Torrance, J. B.; Pannetier, J.; Nazzal, A. I.; Wang, P. W.; Huang, T. C. Synthesis, Crystal Structure, and Properties of Metallic $PrNiO_3$: Comparison with Metallic $NdNiO_3$ and Semiconducting $SmNiO_3$. *J. Solid State Chem.* **1991,** *91,* 225-237.

(11) Medarde, M. L. Structural, Magnetic and Electronic Properties of $RNiO_3$ Perovskites (R

= rare earth). *J. Phys. Condens. Matter* **1997**, *9,* 1679-1707.

(12) Chaloupka, J.; Khaliullin, G. Orbital Order and Possible Superconductivity in $LaNiO_3/LaMnO_3$ Superlattices. *Phys. Rev. B: Condens. Matter Mater. Phys.***2008,** *100,* 016404.

(13) King, P. D. C.; Wei, H. I.; Nie, Y. F.; Uchida, M.; Adamo, C.; Zhu, S.; He, X.; Božović, I.; Schlom, D. G.; Shen, K. M. Atomic-scale Control of Competing Electronic Phases in Ultrathin $LaNiO_3$. *Nat. Nanotechnol*. **2014**, *9,* 443-447.

(14) Boris, A. V.; Matiks, Y.; Benckiser, E.; Frañó, A.; Popovich, P.; Hinkov, V.; Wochner, P.; Castro-Colin, M.; Detemple, E.; Malik, V. K.; Bernhard, C.; Prokscha, T.; Suter, A.; Salman, Z.; Morenzoni, E.; Cristiani, G.; Habermeier, H.-U.; Keimer, B. Dimensionality Control of Electronic Phase Transitions in Nickel-Oxide Superlattices. *Science* **2011,** *332*, 937-940.

(15) Benckiser, E.; Haverkort, M. W.; Brück, S.; Goering, E.; Macke, S.; Frañó, A.; Yang, X.; Andersen, O. K,; Cristiani, G.; Habermeier, H. U.; Boris, A. V.; Zegkinoglou, I.; Wochner, P.; Kim, H.-J.; Hinkov, V.; Keimer, B. Orbital Reflectometry of Oxide Heterostructures. *Nat. Mater*. **2011**, *10,* 189-193.

(16) Gibert, M.; Zubko, P.; Scherwitzl, R.; Íñiguez, J.; Triscone, J. M. Exchange Bias in $LaNiO_3$-$LaMnO_3$ Superlattices. *Nat. Mater.* **2012,** *11,* 195-198.

(17) Lee, A. T.; Han, M. J. Charge Transfer, Confinement, and Ferromagnetism in $LaMnO_3/LaNiO_3$ (001) Superlattices. *Phys. Rev. B : Condens. Matter Mater. Phys.* **2013,** *88,* 035126.

(18) Dong, S.; Dagotto, E. Quantum Confinement Induced Magnetism in $LaNiO_3$-$LaMnO_3$ superlattices. *Phys. Rev. B : Condens. Matter Mater. Phys.***2013,** *87,* 195116.

(19) Hoffman, J.; Tung, I. C.; Nelson-Cheeseman, B. B.; Liu, M.; Freeland, J. W.; Bhattacharya, A. Charge Transfer and Interfacial Magnetism in $(LaNiO_3)_n/(LaMnO_3)_2$ Superlattices. *Phys. Rev. B: Condens. Matter Mater. Phys.* **2013,** *88,* 144411.

(20) Piamonteze, C.; Gibert, M.; Herdler, J.; Rusponi, S.; Brune, H.; Triscone, H.-M. Nolting, F.; Staub, U. Interfacial Properties of $LaMnO_3/LaNiO_3$ Superlattices Grown along (001) and (111) Orientations. *Phys. Rev. B: Condens. Matter Mater. Phys.***2015,** *92,* 014426.

(21) Gibert, M.; Viret, M.; Zubko, P.; Jaouen, N.; Tonnerre, J.-M.; Torres-Pardo, A.; Catalano, S.; Gloter, A.; Stéphan, O.; Triscone, J.-M. Interlayer Coupling through a Dimensionality-induced Magnetic State. *Nat. Commun.* **2016,** *7,* 11227.

(22) Huijben, M.; Martin, L. W.; Chu, Y.-H.; Holcomb, M. B.; Yu, P.; Rijinders, G.; Blank, D. H. A.; Ramesh, R.; Critical Thickness and Orbital Ordering in ultrathin $La_{0.7}Sr_{0.3}MnO_3$ films. *Phys. Rev. B: Condens. Matter Mater. Phys.* **2008,** *78,* 094413.

(23) Chakhalian, J.; Freeland, J. W.; Srajer, G.; Strempfer, J.; Khaliullin, G.; Cezar, J. C.; Charlton, T.; Dalgliesh, R.; Bernhard, C.; Cristiani, G.; Habermeier, H. U.; Keimer, B. Magnetism at the Interface between Ferromagnetic and Superconducting Oxides. *Nat. Phys*. **2006,** *2,* 244-248.

(24) Aruta, C.; Ghiringhelli, G.; Bisogni, V.; Braicovich, L.; Brookes, N. B.; Tebano, A.; Balestrino, G. Orbital Occupation, Atomic Moments, and Magnetic ordering at Interfaces of Manganite Thin Films. *Phys. Rev. B: Condens. Matter Mater. Phys.* **2009,** *80,* 014431.

(25) Son, J.; LeBeau, J. M.; Allen, S. J.; Stemmer, S. Conductivity Enhancement of Ultrathin $LaNiO_3$ Films in Superlattices. *Appl. Phys. Lett.* **2010,** *97,* 202109.

(26) Nogués, J.; Sort, J.; Langlais, V.; Skumryev, V.; Suriñach, S.; Muñoz, J. S.; Baró, M. D. Exchange Bias in Nanostructures. *Phys. Rep*. **2005,** *422*, 65-117.

(27) Sánchez, J. C. R.; Nelson-Cheeseman, B.; Granada, M.; Arenholz, E.; Steren, L. B. Exchange-bias Effect at $La_{0.75}Sr_{0.25}MnO_3/LaNiO_3$ Interfaces. *Phys. Rev. B: Condens. Matter Mater. Phys.***2012,** *85*, 094427.

(28) Peng, J. J.; Song, C.; Li, F.; Cui, B.; Mao, H. J.; Wang, Y. Y.; Wang, G. Y.; Pan, F. Charge Transfer and Orbital Reconstruction in Strain-Engineered $(La,Sr)MnO_3/LaNiO_3$

Heterostructures. *ACS Appl. Mater. Interfaces* **2015,** *7,* 17700-17706.

(29) Ding, J. F.; Lebedev, O. I.; Turner, S.; Tian, Y. F.; Hu, W. J.; Seo, J. W.; Panagopoulos, C.; Prellier, W.; Tendeloo, G. V.; Wu, T. Interfacial Spin Glass state and Exchange Bias in Manganite Bilayers with Competing Magnetic Orders. *Phys. Rev. B: Condens. Matter Mater. Phys.***2013**, *87*, 054428.

(30) Moutis, N.; Christides, C.; Panagiotopoulos, I.; Niarchos, D. Exchange-coupling properties of $La_{1-x}Ca_xMnO_3$ Ferromagnetic/antiferromagnetic Multilayers. *Phys. Rev. B: Condens. Matter Mater. Phys.* **2001**, *64*, 094429.

(31) Balasubramanian, M.; Melendres, C. A.; Mini, S. X-ray Absorption Spectroscopy Studies of the Local Atomic and Electronic Structure of Iron Incorporated into Electrdeposited Hydrous Nickel Oxide Films. *J. Phys. Chem. B* **2000**, *104,* 4300-4306.

(32) Peng, J. J.; Song, C.; Cui, B.; Li, F.; Mao, H. J.; Wang, Y. Y.; Wang, G. Y.; Pan, F. Exchange bias in a Single $LaMnO_3$ Film Induced by Vertical Electronic Phase Separation. *Phys. Rev. B: Condens. Matter Mater. Phys.***2014**, *89*, 165129.

(33) Galdi, A.; Aruta, C.; Orgiani, P.; Adamo, C.; Bisogni, V.; Brookes, N. B.; Ghiringhelli, G.; Schlom, D. G.; Thakur, P. Maritato, L. Electronic Band Redistricution Probed by Oxygen Absorption Spectra of $(SrMnO_3)_n/(LaMnO_3)_{2n}$ Superlattices. *Phys. Rev. B: Condens. Matter Mater. Phys.***2012,** *85*, 125129.

(34) Valencia, S.; Gaupp, A.; Gudat, W.; Abas, L.; Balcells, L.; Cavallaro, A.; Martinez, B.; Palomares, F. J. Mn Valence Instability in $La_{2/3}Ca_{1/3}MnO_3$ Thin Films. *Phys. Rev. B: Condens. Matter Mater. Phys.***2006**, *73*, 104402.

(35) Dass, R. I.; Yan, J.-Q.; Goodenough, J. B. Oxygen Stoichiometry, Ferromagnetism, and Transport Properties of $La_{2-x}NiMnO_{6+\delta}$. *Phys. Rev. B: Condens. Matter Mater. Phys.***2003**, *68*, 064415.

(36) Goodenough, J. B. Magnetism and Chemical Bond. Interscience: New York, 1963.

(37) Das, H.; Waghmare, U. V.; Saha-Dasgupta, T.; Sarma, D. D. Electronic Structure, Phonons, and Dielectric Anomaly in Ferromagnetic Insulating Double Perovskite La_2NiMnO_6. *Phys. Rev. B: Condens. Matter Mater. Phys.* **2008**, *100*, 186402.

(38) Rajeev, K. P.; Shivashankar, G. V.; Raychaudhuri, A. K. Low-Temperature Electronic Properties of a Normal Conducting Perovskite Oxide ($LaNiO_3$). *Solid State Commun.* **1991,** *79,* 591-595.